Connections between the Spring Breakup of the Southern Hemisphere Polar Vortex, Stationary Waves, and Air–Sea Roughness

Chaim I. Garfinkel,* Luke D. Oman,[+] Elizabeth A. Barnes,[#] Darryn W. Waugh,*
Margaret H. Hurwitz,[@] and Andrea M. Molod[&]

* Department of Earth and Planetary Science, The Johns Hopkins University, Baltimore, Maryland
[+] Atmospheric Chemistry and Dynamics Laboratory, NASA/Goddard Space Flight Center, Greenbelt, Maryland
[#] Lamont-Doherty Earth Observatory, Columbia University, Palisades, New York
[@] NASA Goddard Earth Sciences Technology and Research (GESTAR), Morgan State University, Baltimore,
and NASA Goddard Space Flight Center, Greenbelt, Maryland
[&] Global Modeling and Assimilation Office, NASA/Goddard Space Flight Center, Greenbelt, and Earth System
Science Interdisciplinary Center, University of Maryland, College Park, College Park, Maryland

(Manuscript received 30 August 2012, in final form 15 March 2013)

ABSTRACT

A robust connection between the drag on surface-layer winds and the stratospheric circulation is demonstrated in NASA's Goddard Earth Observing System Chemistry–Climate Model (GEOSCCM). Specifically, an updated parameterization of roughness at the air–sea interface, in which surface roughness is increased for moderate wind speeds (4–20 m s^{-1}), leads to a decrease in model biases in Southern Hemispheric ozone, polar cap temperature, stationary wave heat flux, and springtime vortex breakup. A dynamical mechanism is proposed whereby increased surface roughness leads to improved stationary waves. Increased surface roughness leads to anomalous eddy momentum flux convergence primarily in the Indian Ocean sector (where eddies are strongest climatologically) in September and October. The localization of the eddy momentum flux convergence anomaly in the Indian Ocean sector leads to a zonally asymmetric reduction in zonal wind and, by geostrophy, to a wavenumber-1 stationary wave pattern. This tropospheric stationary wave pattern leads to enhanced upward wave activity entering the stratosphere. The net effect is an improved Southern Hemisphere vortex: the vortex breaks up earlier in spring (i.e., the spring late-breakup bias is partially ameliorated) yet is no weaker in midwinter. More than half of the stratospheric biases appear to be related to the surface wind speed biases. As many other chemistry–climate models use a similar scheme for their surface-layer momentum exchange and have similar biases in the stratosphere, the authors expect that results from GEOSCCM may be relevant for other climate models.

1. Introduction

The interaction between the surface and the lowest levels of the atmosphere is a crucial process in nature and in any climate model. The midlatitude surface westerlies are maintained against surface drag by eddy momentum fluxes (Held 1975; Edmon et al. 1980; Vallis 2006, section 12.1). Changes in surface drag can cause meridional shifts of the midlatitude, eddy-driven jet (Robinson 1997; Chen et al. 2007; Kidston and Vallis 2012). The flux of enthalpy into the atmosphere at the bottom of a hurricane regulates subsequent growth of the hurricane (Molod et al. 2013). Increased surface drag leads to more efficient eddy momentum fluxes into the jet core, so that even as the increased roughness is reducing winds, eddies try to counter this effect by more efficiently transporting momentum into the jet (Barnes and Garfinkel 2012).

The exchange of momentum, moisture, and sensible heat between the ocean surface and the atmosphere occurs on spatial and temporal scales far finer than any atmospheric general circulation model (GCM) can directly simulate. Many models therefore rely on Monin–Obukhov similarity theory (MOST) to specify air–sea momentum exchange as a function of bulk winds, temperature, and humidity. However, the coefficients underlying MOST, and specifically those relating the

Corresponding author address: Chaim I. Garfinkel, Department of Earth and Planetary Science, The Johns Hopkins University, Baltimore, MD 21218.
E-mail: cig4@jhu.edu

air–sea roughness to the turbulence in the near-surface flow, are observationally derived. Garfinkel et al. (2011) found that updating these coefficients based on the most recently available observational data for wind speeds between 4 and $20\,\mathrm{m\,s^{-1}}$ leads to improved surface winds over the Southern Ocean in the National Aeronautics and Space Administration (NASA)'s Goddard Earth Observing System Chemistry–Climate Model (GEOSCCM). In addition, they found that the updated parameterization leads to improved zonal surface stress on the ocean and eddy momentum flux convergence aloft. They also mentioned, but did not discuss in detail, the improvement of the Southern Hemispheric (SH) stratospheric circulation. Here, we expand on Garfinkel et al. (2011) and discuss these improvements in the SH stratosphere.

A persistent bias in most chemistry–climate models (CCMs) is the late breakup of the SH stratospheric polar vortex in spring [September–November; cf. chapter 4 of SPARC-CCMVal (2010); Butchart et al. (2011)]. This bias tempers the conclusions that can be drawn from model output data. For example, details regarding the timing of the tropospheric impacts of ozone depletion (e.g., Arblaster and Meehl 2006; Polvani et al. 2011) and the modeled ozone trends in the SH lower stratosphere (e.g., Stolarski et al. 2006) are likely also biased in many models. In the GEOSCCM, the springtime vortex bias has been present in multiple model generations (e.g., Stolarski et al. 2006; Hurwitz et al. 2010) despite improvements to model parameterizations, including the gravity wave parameterization. Hurwitz et al. (2010) showed that the delayed breakup in GEOSCCM is related to overly weak SH lower-stratospheric heat flux in spring, and in particular, to weak stationary planetary waves in the troposphere.

In this paper, we show that a by-product of the improved air–sea roughness parameterization is improved tropospheric stationary waves. Once the tropospheric stationary waves are improved, stratospheric sensible heat flux, and in particular that associated with stationary planetary waves, is improved as well. The polar vortex breaks down earlier in spring, and biases in stratospheric ozone are partially ameliorated. As many other atmospheric CCMs appear to implement a similar air–sea roughness parameterization for momentum exchange as GEOSCCM and base it on similarly old and scant empirical data (e.g., Garfinkel et al. 2011, their Table 1), we expect that the reduction in model bias shown here may be common to other CCMs as well.

This paper is organized as follows. After explaining the methodology in section 2, we document the improvements in stationary waves, heat flux, polar cap temperature, 60°S winds, and stratospheric ozone in sections 3 and 4. We then present a mechanism whereby the change

in air–sea roughness over an essentially zonally symmetric ocean can lead to improved tropospheric stationary waves in section 5. Finally, section 6 demonstrates that more than half of the stratospheric biases appear to be related to the surface wind biases.

2. Methods and data

The GEOSCCM experiments performed use the Goddard Earth Observing System, version 5 (GEOS-5), atmospheric GCM (Rienecker et al. 2008) coupled to a comprehensive stratospheric chemistry module (Pawson et al. 2008). The model has 72 vertical layers, with a model top at 0.01 hPa, and all simulations discussed here were performed at 2° latitude × 2.5° longitude horizontal resolution. A 25-yr run at 1° × 1.25° horizontal resolution without interactive stratospheric chemistry has been performed to test sensitivity to resolution, and results are qualitatively similar (not shown). SPARC-CCMVal (2010) grades highly the representation of the Southern Hemisphere stratosphere by an earlier version of GEOSCCM as compared to observations and to the multimodel mean of an ensemble of CCMs.

Details of the surface-layer scheme used in GEOSCCM can be found in the appendix of Helfand and Schubert (1995), and a description of the update of the air–sea roughness parameterization can be found in Garfinkel et al. (2011). Briefly, Garfinkel et al. (2011) showed that the local effect of updating the parameterization was 1) to increase the roughness and the momentum exchange coefficient and 2) to decrease surface wind speed, over the oceanic regions where the wind speed exceeds $4\,\mathrm{m\,s^{-1}}$. Here, the effect of updating the air–sea roughness parameterization on the stratospheric circulation is evaluated in the GEOSCCM. The air–sea roughness parameterization in the CONTROL (i.e., lower roughness) simulation is different from that in the UPDATED [i.e., updated as in Garfinkel et al. (2011) with higher roughness] simulation; all other boundary conditions and model settings are identical in the two simulations. Three 30-yr "CONTROL" and 30-yr "UPDATED" model integrations were performed. While the three ensemble members differ in their gravity wave drag scheme [one follows Rienecker et al. (2008), while two follow Molod et al. (2012)], the key results presented in this paper are insensitive to the choice of gravity wave drag scheme. Thus, in the discussion of our results, we do not distinguish between the three ensemble members.

Greenhouse gas and ozone-depleting substance concentrations represent the year 2005 in all experiments discussed here. The sea surface temperatures in the years 1980–2010 force each 30-yr pair. Variability related to the solar cycle and volcanic aerosols are not

considered. The parameterization of enthalpy fluxes at the air–sea interface is held fixed between UPDATED and CONTROL. The key point is that these simulations isolate the impact of updating the air–sea roughness parameterization for momentum.

a. Validation

NASA's Modern-Era Retrospective Analysis for Research and Applications (MERRA; Rienecker et al. 2011) is used to validate the model's height, eddy fluxes, and zonal wind away from the surface; results are nearly identical when we use 40-yr European Centre for Medium-Range Weather Forecasts (ECMWF) Re-Analysis (ERA-40; Uppala et al. 2005). The model's ozone is compared to the patched and interpolated satellite-based product available online (at http://www.bodekerscientific.com/data/total-column-ozone) [updated from Bodeker et al. (2001, 2005)]. Modeled surface winds and surface stress are validated against version 2 of the Goddard Satellite-Based Surface Turbulent Fluxes (GSSTF) data [available at http://disc.sci.gsfc.nasa.gov/precipitation/data-holdings/access/gsstf2.0.shtml and described in Chou et al. (2003)]. For ozone and quantities derived from MERRA, we begin the validation period in 1989 since the model is forced with 2005 ozone-depleting substances and we wish to restrict our analysis to observed years with comparable levels of ozone-depleting substances.

b. Diagnostics

In section 5, we will use a vorticity budget to diagnose the role of eddies in establishing a tropospheric zonal wavenumber-1 (hereafter wave-1) response to the updated air–sea drag. Here, we introduce the budget used to demonstrate this effect. Barnes and Hartmann (2010a, hereafter BH10) and Barnes and Hartmann (2010b) show that the interactions between temporal eddies and the time mean flow in zonally confined regions can be diagnosed quantitatively by using the vorticity budget (Holton 2004):

$$\frac{\partial \hat{\zeta}}{\partial t} = [-(\overline{\zeta}+f)\mathbf{\nabla}\cdot\hat{\mathbf{u}} - \hat{\zeta}\mathbf{\nabla}\cdot\overline{\mathbf{u}}]_{\text{stretching}} + [-\mathbf{\nabla}\cdot(\hat{\mathbf{u}\zeta})]_{\text{eddy}}$$
$$+ [-\hat{\mathbf{u}}\cdot\mathbf{\nabla}(\overline{\zeta}+f) - \overline{\mathbf{u}}\cdot\mathbf{\nabla}\hat{\zeta}]_{\text{wave}}$$
$$+ \{-\mathbf{\nabla}\cdot[\overline{\mathbf{u}}(\overline{\zeta}+f)]\}_{\text{clim}} + \mathcal{F}.$$

$$(1)$$

The overbar represents the time mean and the caret represents the deviation from the time mean, ζ is the vorticity, f is the Coriolis parameter, $\mathbf{u}$ is the vector wind, and $\mathcal{F}$ is the drag as applied to vorticity and is proportional to the surface stress [e.g., section 7 of Barnes and Garfinkel (2012)]. BH10 demonstrate that when the

vorticity forcing terms in upper levels project onto vorticity anomalies in lower levels, lower-level vorticity anomalies can be maintained against damping. This budget was also used to demonstrate that eddies respond to an external forcing in Garfinkel and Hartmann (2011). See BH10 for more details.

The vorticity budget is used here to diagnose the role of tropospheric eddies in the tropospheric response to the updated surface drag. The terms in the vorticity budget are computed for the CONTROL and UPDATED runs. The difference in the forcing terms between the UPDATED and the CONTROL runs represents the generation of tropospheric vorticity anomalies in response to increased surface drag. Specifically, we will show that a wave-1 surface stress anomaly $\mathcal{F}$ is balanced by the other terms in the budget.

A two-tailed Student's t test is used to assess statistical significance where indicated. Each year is taken as 1 degree of freedom, except when we discuss the high-frequency poleward eddy momentum flux where each month is taken as 1 degree of freedom. (Quasi-) stationary heat flux is computed from $\overline{v_{\text{SO}}^* T_{\text{SO}}^*}$, where v_{SO}^* is the deviation of the meridional wind from the zonal mean averaged over September and October (SO), T_{SO}^* is like v_{SO}^*, but for temperature, and the overbar denotes a zonal average. Heat flux is used as a proxy for wave activity flux. High-frequency eddy momentum fluxes are computed by applying a 7-day high-pass ninth-order Butterworth filter applied separately to the meridional and zonal velocities before computing their product.

We now address the impact of the change in the air–sea roughness parameterization on bulk quantities in the model.

3. Improvements in the zonally averaged circulation

We first focus on the bias in polar cap temperature (75°S and poleward) of the CONTROL climate and its improvement upon updating the air–sea roughness parameterization. The climatological polar cap temperature in observations and in the model are shown in Figs. 1a and 1b, and the difference between the two climatologies is shown in Fig. 1c. In the CONTROL climate, modeled temperatures are too warm in autumn and winter yet are too cold in spring. When we update the air–sea roughness parameterization, we find that while the bias during winter is unchanged, the biases during fall and spring are reduced (Fig. 1d). In the lower stratosphere, the springtime bias is reduced by around one-third.

Subpolar (60°S) zonal-mean zonal wind is also improved when we update the air–sea roughness. The climatological subpolar zonal winds in observations and in the model
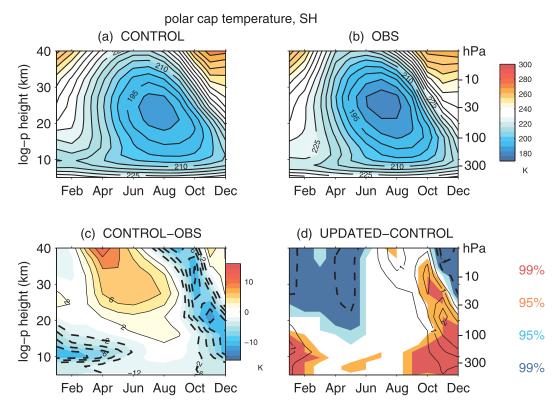
FIG. 1. Polar cap temperature (area-weighted average, 75°S and poleward) evolution over the course of the year in (a) CONTROL, (b) reanalysis data, (c) CONTROL minus reanalysis, and (d) UPDATED minus CONTROL. The contour interval is 5 K in (a),(b), 2 K in (c), and 0.5 K in (d). Regions with anomalies significant at the 95% (99%) level are orange for positive anomalies or light blue for negative anomalies (red or dark blue, respectively) in (d). The zero contour is omitted.

are shown in Figs. 2a and 2b and the difference between the two climatologies is shown in Fig. 2c. In the CONTROL climate, winds are too strong in spring and summer. When we update the air–sea roughness parameterization, we find that westerlies weaken in all seasons in the troposphere and lower stratosphere, but the effect is strongest in SH spring. In the middle and upper stratosphere, winds are decreased only in spring and summer. The biggest easterly anomalies occur where the CONTROL experiment is biased toward too-strong westerlies (in late spring and early summer). Note that the midwinter vortex is not significantly affected by the change in the air–sea roughness parameterization, but the vortex breaks up earlier in spring. The earlier vortex breakup is clearly shown in the timing of the springtime transition to easterlies in the SH at 60°S, one of the metrics identified by SPARC-CCMVal (2010). Figure 3b shows that by this metric as well, GEOSCCM is now improved by approximately one week near 10 hPa (33% of the bias), though model biases do still exist.[1]

Zonally averaged polar cap (75°S and poleward) column ozone is also improved in GEOSCCM in late spring (Fig. 3c). In November and December, there is significantly more ozone in the SH polar region. More than half of the bias in GEOSCCM in these months is eliminated by the updated air–sea roughness parameterization, though the large variability in the observational data complicates our interpretation. The improvement in spring column ozone is consistent with the earlier vortex breakup. The high ozone bias of the model (e.g., Pawson et al. 2008) complicates the interpretation of the results in January. The change in May and June appears to be related to a change in transport across the polar vortex: column ozone is significantly increased between 30° and 60°S (not shown). There is no net effect if we average from 30°S to the pole. A detailed investigation of the change in late fall is beyond the scope of this work.

Interannual variability of the spring vortex breakup is also improved. To demonstrate this, we show the standard deviation of polar cap column ozone among the 90 years in CONTROL and in UPDATED in Fig. 3d. There is too little interannual variability in CONTROL. In other words, the breakup date of the ozone hole is too tightly clustered around the same time period (which in

---

[1] The magnitude of this bias is much smaller at 1° × 1.25° horizontal resolution (not shown).

60° zonal wind, SH
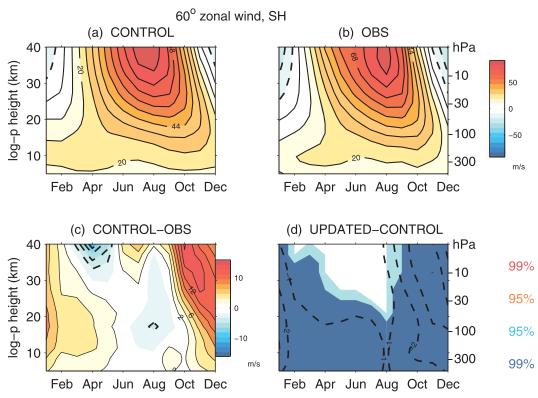

FIG. 2. As in Fig. 1, but for 60°S zonal wind evolution over the course of the year. The contour interval is $8\,\mathrm{m\,s^{-1}}$ in (a),(b), $2\,\mathrm{m\,s^{-1}}$ in (c), and $1\,\mathrm{m\,s^{-1}}$ in (d).

turn is also biased as shown in Fig. 3c). In contrast, more interannual variability is present in spring in UPDATED, though the springtime peak in variability is still delayed as compared to observations. In summary, the zonally averaged circulation, and in particular polar cap temperature, 60°S zonal wind, and column ozone, is improved in midspring through early summer by updating the air–sea roughness parameterization.

4. Improvements in the zonally asymmetric circulation

We now discuss zonally asymmetric improvements in September–October. We focus on September–October because it precedes the largest improvements in the zonally averaged stratospheric circulation (Hurwitz et al. 2010). Figures 4 and 5 show that surface wind speed, upper-tropospheric zonal wind, upper-tropospheric height, and column ozone are all improved by the updated parameterization in September–October. As discussed in Garfinkel et al. (2011), wind speed at the surface is improved. This can be seen by noting that the regions of largest bias in the CONTROL run in Fig. 4b have opposite changes in Fig. 4c. In addition, the pattern of the change resembles zonal wave 1: winds are decelerated

most strongly in the Pacific sector (Fig. 4c). Aloft, the bias in the model, and the improvement upon updating the air–sea roughness parameterization, also resemble a strong wave-1 pattern (Figs. 4d–f). Associated with the reduction in zonal wind over the Southern Ocean is a subpolar high and subtropical low (Figs. 5a,b) by geostrophy. Since the reduction in zonal wind is concentrated in the Pacific sector, the anomalous ridge is strongest in this region.

To show the vertical structure of the height anomalies, we compute the deviation of height from the zonal mean (i.e., the zonally asymmetric component), weight it by the square root of the air density [as in Matsuno (1970) and in section 12.3.1 of Holton (2004)], and then plot the result in Fig. 6. Stationary planetary (in particular wave-1) waves are too weak in CONTROL (Figs. 6b,c,e), but the bias is partially ameliorated in UPDATED throughout the troposphere and stratosphere (cf. the color hues in Figs. 6d and 6e). The improvement generally resembles wave-1; consistent with Figs. 5a and 5b, positive height anomalies are larger in the Pacific sector in the troposphere (Fig. 6f). In the stratosphere, the anomaly has westward tilt with height, which is indicative of enhanced wave activity flux into the stratosphere.
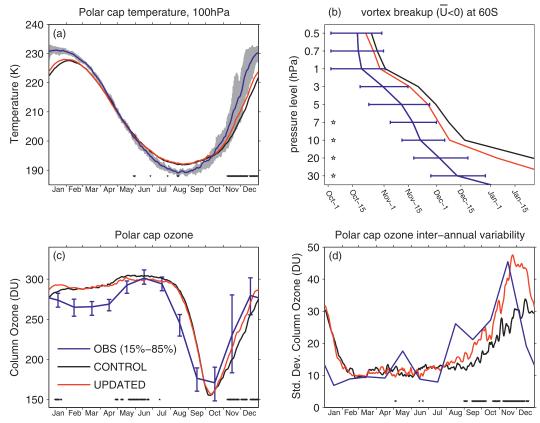
FIG. 3. Evolution of (a) polar cap temperature at 100 hPa, (b) the date on which 60°S zonal wind reaches $0\,\mathrm{m\,s^{-1}}$ (i.e., the vortex breakup), (c) polar cap column ozone, and (d) variability in polar cap column ozone, in the UPDATED, CONTROL, and reanalysis data. The range of observational variability is indicated with gray shading or error bars. Days in which UPDATED and CONTROL are significantly different from each other at the 95% level are designated with a star below the curves or to the left of the curves. The polar cap average is defined as the area-weighted average 75°S and poleward. Monthly averaged data is used for the observations for (c),(d), and daily data are used for the observations for (a),(b). For (d), an F test is used to assess significance.

Zonally asymmetric improvements in ozone are also present in September–October. Namely, the bias in column ozone, as well as its improvement upon increasing the air–sea roughness, also bears a wave-1 pattern (Figs. 5c,d). A comparison of the phasing of the ozone improvement in Figs. 5c and 5d and the height improvement in Fig. 6f suggests that the geostrophic flow associated with the height improvement can, by advecting ozone, lead to improved ozone as well. Namely, poleward motion south of the Indian Ocean advects ozone-rich subpolar air poleward, while equatorward motion south of South America advects ozone-poor polar air equatorward. Even though the zonally averaged improvements in ozone do not begin until November (Fig. 2c), zonally asymmetric improvements are present earlier.

Next, we consider the change in heat flux (Fig. 7). In the stratosphere, the model has too little heat flux (Figs. 7a,b). This bias in the stratosphere is partially ameliorated when we update the air–sea roughness

parameterization (Fig. 7c).[2] Nearly all of the bias in the model, as well as the improvement in UPDATED, is associated with the stationary waves as opposed to the transient waves (Figs. 7d–f). It is not surprising that the improvement in stationary wave heat flux and in height should be linked. Garfinkel et al. (2010) and Smith and Kushner (2012) argue that if an anomalous ridge is collocated with a ridge of the climatological planetary wave pattern (as is evident in the troposphere in Fig. 6f), then tropospheric upward wave activity flux will be enhanced. Figure 8 confirms that the change in heat flux in the stratosphere is associated almost entirely with wave 1. However, the too-low heat flux bias in GEOSCCM discussed in Hurwitz et al. (2010) is not removed entirely. In the troposphere as well (where synoptic transient heat

---

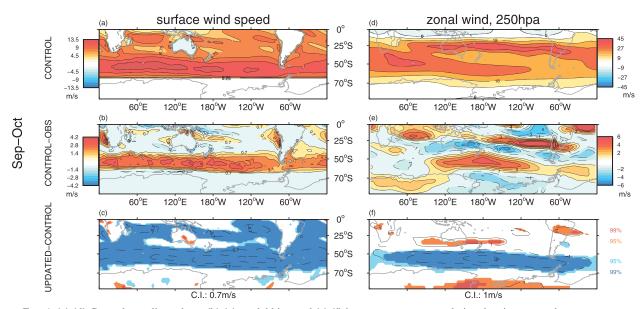[2] The magnitude of this bias is much smaller at $1° \times 1.25°$ horizontal resolution (not shown).

FIG. 4. (a),(d) Control run climatology, (b),(e) model bias, and (c),(f) improvement upon updating the air–sea roughness parameterization in (a)–(c) surface wind speed, and (d)–(f) 250-hPa zonal wind, during September and October. The contour intervals are 2.25 m s^{-1} in (a), 0.7 m s^{-1} in (b),(c), 9 m s^{-1} in (d), and 1 m s^{-1} in (e),(f). Regions with anomalies significant at the 95% (99%) are light (dark) red or blue in (e) and (f), with red denoting positive anomalies and blue denoting negative anomalies. The zero contour is omitted and negative contours are dashed and thick.

flux dominates stationary and planetary wave heat flux climatologically), planetary wave heat flux is improved (Fig. 9). In particular, wave-1 heat flux between 50° and 70°S is significantly increased (Fig. 9d). We defer a discussion of the changes for synoptic wavenumbers in the troposphere and for forecasting skill, and a comparison of our results to those of Branscome et al. (1989), for future work.

In summary, the updated air–sea roughness parameterization leads to a strong wave-1 response in September–October. Zonally asymmetric height, zonal wind, and eddy heat flux are all improved. The improved heat flux in

September–October then drives the zonally symmetric improvements in the late spring and early summer stratospheric circulation discussed in section 3.

5. How does surface roughness impact stationary waves?

We now seek to mechanistically explain the origin of these zonally asymmetric improvements in the upper-tropospheric and stratospheric circulation. In particular, we seek to answer the following questions.
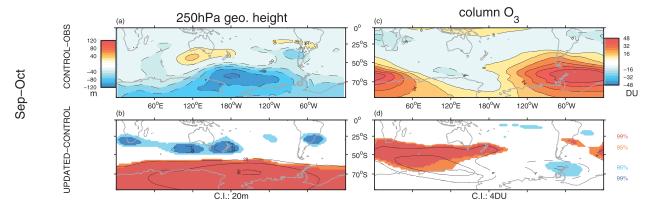

FIG. 5. (a),(c) Model bias and (b),(d) improvement upon updating the air–sea roughness parameterization in (a),(b) 250-hPa height, and (c),(d) column ozone, during September and October. The contour intervals are as follows: 20 m in (a),(b), 8 Dobson units (DU) in (c), and 4 DU in (d). Regions with anomalies significant at the 95% (99%) are light (dark) red or blue in (c),(d), with red denoting positive anomalies and blue denoting negative anomalies. The zero contour is omitted and negative contours are dashed and thick.
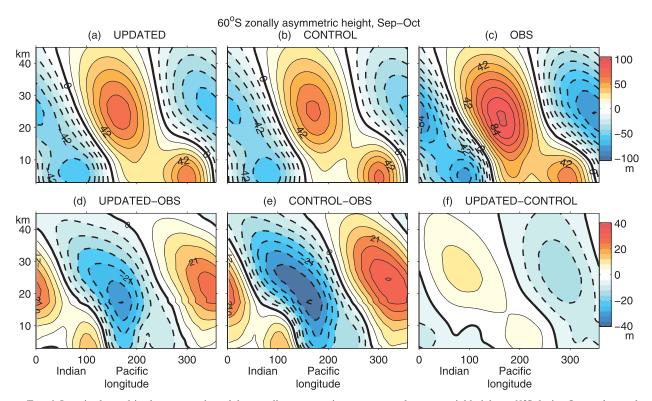
FIG. 6. Longitude vs altitude cross section of the zonally asymmetric component of geopotential height at 60°S during September and October in (a) UPDATED, (b) CONTROL, (c) reanalysis data, (d) UPDATED minus reanalysis, (e) CONTROL minus reanalysis, and (f) UPDATED minus CONTROL. The contour interval is 15 m for (a)–(c) and 7.5 m for (d)–(f). Height has been weighted by $\sqrt{p/p_s}$, the ratio of the pressure at each level to the surface pressure, as described in the text. Additional panels are shown in order to ease comparison with Fig. 7 of Hurwitz et al. (2010). The zero contour is thick.

(i) What is the mechanism whereby a change in air–sea roughness over the essentially zonally symmetric Southern Ocean can lead to a wave-1 tropospheric response?

(ii) What controls the phase of the wave-1 pattern?

One might hypothesize that the response to drag is proportional to the local climatological wind speed and thus bears a slight zonal wave-1 structure as the underlying Southern Ocean winds bear a slight wave-1 structure (cf. Fig. 4a; such a prediction follows from running the surface layer scheme offline from the rest of the model.). However, the strongest climatological surface winds are in the Indian Ocean sector, while the strongest response is in the Pacific sector and not in the Indian Ocean sector (Fig. 4a vs Fig. 4c). Thus, a simple scaling argument based on the climatological wind speed fails to predict the response. The rest of this section presents a more plausible mechanism as to how the change in roughness can create a wave-1 anomaly in the troposphere.

As mentioned in the introduction, Barnes and Garfinkel (2012) note that as drag on winds is increased in a barotropic model, eddy momentum fluxes into the jet core are

enhanced if the drag is quadratic (or cubic, once one accounts for the increase in the momentum exchange coefficient with wind speed) in wind speed as in GEOSCCM. Even as the increased roughness is reducing winds, eddies try to counter this effect by more efficiently transporting momentum into the jet. This behavior is also evident in Fig. 3 of Kidston and Vallis (2012).

In the SH, the region of eddy momentum flux is zonally asymmetric in September–October, as seen in Fig. 10a. In particular, Fig. 10a shows that more high-frequency eddy momentum flux convergence (EMFC) occurs in the Indian Ocean sector than in the Pacific sector [consistent with Barnes and Hartmann (2010b)]. The wave-1 zonal asymmetry is especially strong during SH winter, but it is present in September–October and in the annual average as well. It is also present in other diagnostics of storm tracks (e.g., Hoskins and Hodges 2005, their Figs. 2 and 11; Chang et al. 2013, their Fig. 1).

The bias in EMFC in CONTROL, and the improvement upon increasing the surface roughness, also bears a zonally asymmetric wave-1 pattern (Figs. 10c,e). In the Indian Ocean sector, eddies react strongly to the weakening of the jet by enhanced roughness (Fig. 10e).
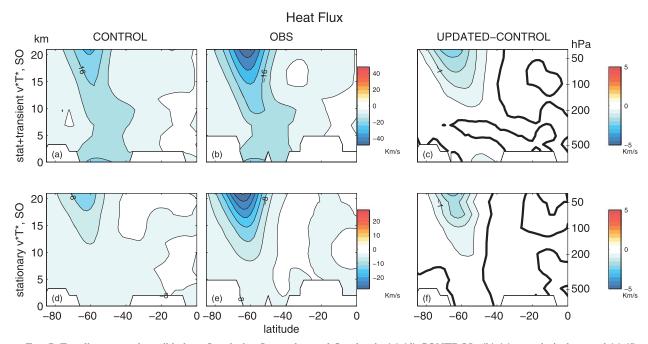
Heat Flux

FIG. 7. Zonally averaged sensible heat flux during September and October in (a),(d) CONTROL, (b),(e) reanalysis data, and (c),(f) UPDATED minus CONTROL. (a)–(c) The total heat flux and (d)–(f) stationary waves only are shown. The difference upon increasing the roughness is shown in (c), (f). The contour interval is $8\,\mathrm{K\,m\,s^{-1}}$ in (a),(b), $4\,\mathrm{K\,m\,s^{-1}}$ in (d),(e), and $0.5\,\mathrm{K\,m\,s^{-1}}$ in (c),(f). The zero contour is thick in (c),(f).

In the Pacific sector, however, the torque due to the eddies is weak and so the decrease in zonal wind because of enhanced roughness is larger there. In other words, a simple scaling argument applied to the climatological eddies (rather than the climatological surface wind speed) can explain the response of eddies to increased surface drag: the response of eddies to drag is proportional to the local intensity of eddy activity and thus features a pronounced maxima in the Indian Ocean sector. Because of this, the strongest change in zonal wind due to eddies is in the Indian Ocean sector. Finally, because eddies act to accelerate the jet, they counteract the effect of increased friction most strongly in the Indian Ocean sector.

A close examination of Fig. 10e suggests that the EMFC is positive only on the equatorward flank of the Indian Ocean sector jet and not on the poleward flank of the jet—the change resembles a meridional dipole—and so it is not clear whether the net effect in the Indian Ocean sector is to accelerate or decelerate the jet. There are two points to bear in mind when considering this issue. First, the jet itself shifts equatorward in response to surface friction [see Fig. 4f, Robinson (1997), and Kidston and Vallis (2012)]. The equatorward shift is amplified here because the polar stratospheric vortex is weakened and a weakened vortex tends to shift tropospheric jets equatorward [see Fig. 1, and also Garfinkel et al. (2012), and the references therein]. We therefore

should expect an equatorward shift in EMFC. Second, we have analyzed the total zonally asymmetric forcing of vorticity which was introduced in section 2b, and we find that the subsequent interaction of the eddies with the mean state 1) is more clearly associated with an acceleration in the Indian Ocean sector poleward of the jet core and 2) is stronger than the deceleration because of the high-frequency eddies in this region. This effect is easily seen in Fig. 11, which shows the upper-tropospheric height, vorticity, and total forcing (azonal plus zonal) of vorticity in the SH averaged from 50° to 70°S. The total forcing of vorticity is defined as the right-hand side of Eq. (1) except for $\mathcal{F}$, the direct effect of the frictional forcing. The direct effect of increasing roughness is to increase (i.e., a positive anomaly of) subpolar vorticity and geopotential height because of geostrophy (red and black curves in Fig. 11). The eddy forcing counteracts this change and reduces vorticity in the zonal average (blue curve in Fig. 11), but the primary reduction is in the Indian Ocean sector. The eddy fluxes are weakest climatologically in the Pacific sector as well (e.g., Fig. 10a). The net effect is that the height and vorticity response to increased roughness is strongest in the Pacific sector where the eddy fluxes are weakest.

The changes in eddy momentum flux convergence aloft imply anomalous surface stress, as $\partial\overline{u^*v^*}/\partial y$ must balance the removal of surface momentum by friction
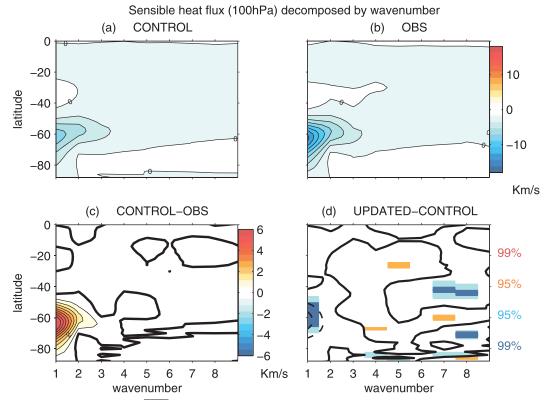
FIG. 8 As in Fig. 1, but for $\overline{v^* T^*}$ at 100 hPa during September–October as a function of zonal wavenumber. The contour interval is $2\,\mathrm{K\,m\,s^{-1}}$ in (a),(b) and $2/3\,\mathrm{K\,m\,s^{-1}}$ in (c),(d). The zero contour is thick.

for a steady-state surface jet (Held 1975; Vallis 2006, section 12.1). Figures 10d,f show that zonal surface stress is also improved with the updated surface roughness as discussed in Garfinkel et al. (2011). In addition, it is clear that the change in surface stress bears a wave-1 signature. Furthermore, the phase of the wave-1 pattern is different than that for, for example, height or zonal wind, but is similar to that of EMFC; namely, the largest change in surface stress is in the Atlantic/Indian Ocean sector and not in the Pacific Ocean sector. It is remarkable that the changes in surface stress and eddy momentum flux convergence balance each other nearly perfectly even without performing a zonal average (cf. Figs. 10e and 10f). Hence, we can explain the differences in phasing between the surface stress and eddy flux changes (which are largest in the Indian Ocean sector) and the zonal wind changes (which are largest in the Pacific sector): the surface stress changes most strongly where the EMFC change is largest, while the surface wind changes most strongly where the EMFC change is smallest.

The schematic in Fig. 12 summarizes the observed changes in the troposphere. Climatologically, the drag and eddies balance each other such that there are westerlies over the Southern Ocean. When we update the air–sea roughness parameterization, we increase the drag in a nearly zonally symmetric manner (and if anything, the change is strongest in the Indian Ocean sector if the air–sea roughness scheme is run offline). This is represented by the orange easterly arrows in both the Indian Ocean and Pacific sectors. However, eddies act to mitigate this easterly anomaly; this effect is represented by dark blue arrows. Eddies are stronger climatologically in the Indian Ocean sector, and thus, the dark blue arrow is longer in the Indian Ocean sector than in the Pacific sector. The net effect is that the deceleration of the wind, which is represented with a purple-gray arrow, is larger in the Pacific sector than in the Indian Ocean sector.

If we revisit the changes in zonal wind and height in Figs. 4a–f and 5a–b, it is clear that the zonal wind reduction at the surface and aloft because of increased roughness is strongest in the Pacific sector. Eddies accelerate the flow throughout the midlatitude Indian Ocean sector [as suggested by the simpler experiments of Barnes and Garfinkel (2012)], but not in the Pacific Ocean sector; hence, increased surface roughness leads to a wave-1 response.
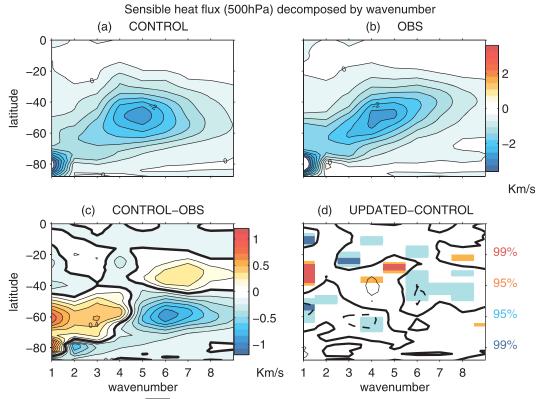
Sensible heat flux (500hPa) decomposed by wavenumber

FIG. 9. As in Fig. 8, but for $\overline{v^*T^*}$ at 500 hPa during September–October. The contour interval is $0.4\,\mathrm{K\,m\,s^{-1}}$ in (a),(b) and $0.1333\,\mathrm{K\,m\,s^{-1}}$ in (c),(d). The zero contour is thick.

Now that we have mechanistically explained the origin of the wave-1 pattern for the zonal wind change (because the eddies do not compensate as strongly in the Pacific sector), the rest of the response follows simply. The anomalous ridging is stronger in the Pacific sector because of geostrophy. This anomalous ridge then affects the stationary waves (Figs. 6–8) and leads to increased wave driving of the vortex. The increased heat flux entering the stratosphere in September–October causes an earlier breakup of the stratospheric vortex. The key point is that because eddies are less effective at counteracting the effect of enhanced ocean roughness in the Pacific sector as compared to the Indian Ocean sector, the net response will bear a wave-1 structure.

This mechanism is consistent with the timing of the improvement in stationary waves and in polar cap temperature. The midwinter SH vortex appears to be too strong to be greatly affected by enhanced tropospheric resolved waves (Charney and Drazin 1961; Scott and Haynes 2002; Taguchi and Yoden 2002). Therefore, it is to be expected that the late-breakup bias can be alleviated while not exacerbating the midwinter bias once resolved stationary waves are improved. In addition, this mechanism would suggest that the fall spinup of the

vortex would not be affected by the updated air–sea roughness parameterization. The mechanism relies on the existence of stationary waves in the troposphere, and in February–April (when the vortex spins up), the tropospheric circulation is more zonally symmetric [not shown, but similar to Fig. 2 of Hoskins and Hodges (2005)].

Note that this mechanism appears disconnected from the barotropic governor of James and Gray (1986) and James (1987). Wave-1 stationary waves are the cause of the increased wave driving of the vortex and not higher-frequency synoptic waves as might be expected from an argument involving baroclinic instability.

In summary, Barnes and Garfinkel (2012) show that eddies can change so as to counteract the effects of increased friction on the mean flow; that is, eddies act to accelerate the jet. The mechanism we present takes this just one step further: eddies are effective at compensating for the increased surface roughness mainly where high-frequency eddies are strongest climatologically (i.e., in the storm tracks). Because the storm tracks have a wave-1 pattern in September–October in the SH, the response to increased surface roughness will have a wave-1 structure as well.
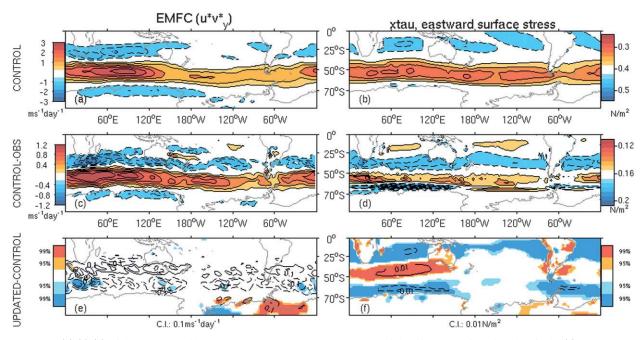
FIG. 10. (a),(c),(e) High-frequency eddy momentum flux convergence pressure weighted between 150 and 200 hPa in the (a) CONTROL run, (c) CONTROL minus observations, and (e) UPDATED minus CONTROL. Contour interval is $0.75 \, \mathrm{m \, s^{-1} \, day^{-1}}$ in (a), $0.3 \, \mathrm{m \, s^{-1} \, day^{-1}}$ in (c), and $0.15 \, \mathrm{m \, s^{-1} \, day^{-1}}$ in (e). (b),(d),(f) As in (a),(c),(e), but for eastward surface stress. Contour interval is $5 \times 10^{-2} \, \mathrm{N \, m^{-2}}$ in (b), $2 \times 10^{-2} \, \mathrm{N \, m^{-2}}$ in (d), and $10^{-2} \, \mathrm{N \, m^{-2}}$ in (f). Regions with anomalies whose statistical significance exceeds 95% are in color in (e),(f). The zero contour is omitted and negative contours are dashed. For this figure only, we show the annual average, as the September–October average is very noisy (though qualitatively similar) for these quantities.

6. Stratospheric improvement upon removing entirely the surface wind bias

In all previous sections of this paper, we have considered the changes in the model upon updating the air–sea roughness coefficients to match recent observations (e.g., Garfinkel et al. 2011, their Fig. 2). However, updating the air–sea roughness parameterization led to only a 45% reduction of the original bias in surface wind speed. Specifically, the bias in zonally averaged Southern Ocean surface winds in the CONTROL experiment is $2.75 \, \mathrm{m \, s^{-1}}$, but the reduction shown in Garfinkel et al. (2011) and discussed here is only $1.2 \, \mathrm{m \, s^{-1}}$. The subsequent stratospheric improvement is 25%–50% of the original stratospheric bias.

In this section, we demonstrate that if the surface wind speed bias was removed entirely, 50%–100% of the stratospheric biases would be alleviated. We have performed a 27-yr sensitivity model experiment where the drag at the air–sea interface is increased far beyond what is observationally or theoretically justified, such that the surface wind speeds become realistic over the Southern Ocean. This is achieved by doubling the drag coefficient [C_D in Eq. (2) of Garfinkel et al. (2011)] from 45°S and poleward after MOST has been applied, rather than updating the air–sea roughness coefficients as in Table 2

of Garfinkel et al. (2011). Figure 13 shows the stratospheric seasonal evolution in these experiments. The bias in column ozone in SON is removed, while the midwinter vortex is unchanged. Overall, the decrease in the model biases in the stratosphere are approximately double that in the more realistic experiments shown in
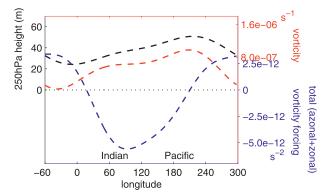

FIG. 11. Averaged 250-hPa height (m; Fig. 10d), vorticity ($\mathrm{s^{-1}}$) averaged from 150 to 200 hPa, and the total (azonal + zonal) vorticity forcing ($\mathrm{s^{-2}}$) averaged from 150 to 200 hPa (both the transient eddies themselves and the interaction of transient eddies with the mean flow) for UPDATED minus CONTROL. Each quantity has been averaged between 50° and 70°S. Heavy smoothing has been applied, though results are qualitatively similar without smoothing.

FIG. 12. Schematic of the response to increased surface roughness over the Southern Ocean. When the roughness is updated, drag is increased in a nearly zonally symmetric manner, as indicated by the orange easterly arrows in both the Indian Ocean and Pacific sectors. However, eddies (represented by dark gray arrows) act to mitigate this easterly anomaly. Because eddies are stronger climatologically, and also in response to an external forcing, in the Indian Ocean sector, the dark blue arrow is longer in the Indian Ocean sector than in the Pacific sector. The net effect is that the deceleration of the wind, which is represented with a purple–gray arrow, is larger in the Pacific sector than in the Indian Ocean sector.

Fig. 3, so that there appears to be a linear relationship between improving the surface wind speed bias and the stratospheric SON biases.

These experiments show that in a sensitivity (i.e., supertuned) experiment in which the surface winds are forced to become realistic, the improvement in the stratospheric circulation is even more pronounced than when the available air–sea roughness data are used to update the model. These experiments suggest that additional, observationally justified, improvements to the model's air–sea drag parameterization that result in further improvements to the surface wind speed may also result in further improvements to the stratospheric flow.

7. Discussion and conclusions

An update to the air–sea roughness parameterization in NASA's Goddard Earth Observing System Chemistry–Climate Model (GEOSCCM) leads to a decrease in model biases in both the troposphere and stratosphere. More than half of the model's SH stratospheric biases appear to be related to air–sea roughness and surface wind speed biases. Increased surface roughness leads to an improved stationary wave pattern and enhanced upward wave activity flux entering the stratosphere in September and October. The increased wave driving leads to a more realistic Southern Hemisphere vortex: the vortex is no weaker in midwinter yet breaks up earlier in
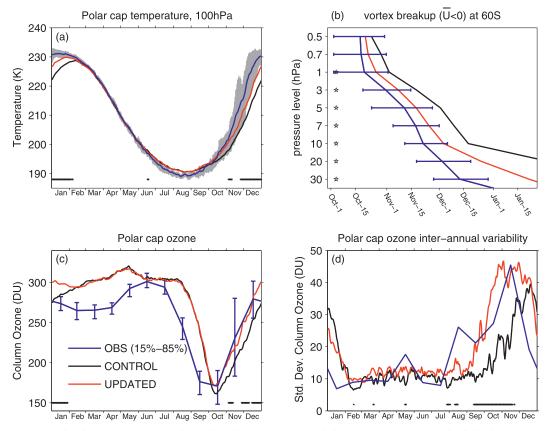

FIG. 13. As in Fig. 3, but for the experiment in which the surface drag is increased beyond that which is justified by the available data on the air–sea interface, but in which the surface wind speed bias is entirely removed.

spring, which leads to improved polar cap temperatures and ozone from November through January.

A possible mechanism whereby increased surface roughness leads to a zonally asymmetric stationary wave response is presented. Barnes and Garfinkel (2012) showed that increased drag on the mean flow leads to increased eddy momentum flux convergence to the jet core. Here, we demonstrate that this effect occurs primarily in regions where eddies are strong climatologically (i.e., in the Indian Ocean sector and not the Pacific sector of the Southern Hemisphere). The wave-1 pattern of the eddy momentum flux convergence anomaly leads to a wave-1 pattern of the reduction in zonal wind and, by geostrophy, to a wave-1 geopotential height response. As the wave-1 anomaly is in phase with the climatological tropospheric stationary waves, wave-1 heat flux in the troposphere and the stratosphere is increased. Future work with simpler models is necessary to confirm this mechanism.

Other studies have examined the impact of changes in other parameterizations on vortex biases. For example, McLandress et al. (2012) find that by parameterizing the orographic gravity waves associated with subgrid scale islands in the Southern Ocean, the delayed vortex breakup in the Canadian Middle Atmosphere Model (CMAM) is improved. However, they note that it is not possible to simultaneously hasten the springtime breakup without weakening the midwinter vortex. In contrast, we find that this change in air–sea roughness weakens the vortex in spring and early summer only. As resolved waves tend to only weakly influence the vortex in midwinter (Taguchi and Yoden 2002, and references therein), it is perhaps to be expected that an improvement involving resolved waves (i.e., air–sea roughness) would be more effective in alleviating the late-breakup bias without exacerbating the midwinter bias. Furthermore, Hurwitz et al. (2010) attribute the delayed breakup in GEOSCCM to overly weak SH lower-stratospheric heat flux, and in particular, to weak stationary planetary waves in the troposphere, and here we have shown that the updated roughness parameterization leads to improved stationary waves in the midtroposphere (cf. Figs. 6 and 9). Finally, the newest implementation of the GEOSCCM includes orographic gravity wave drag associated with isolated small mountains in the subpolar SH (Molod et al. 2012, section 2.4), but the model biases persist. While an unresolved wave source might be important in other models (e.g., CMAM), an improved representation of resolved planetary waves in both the troposphere and stratosphere appears to be more important for GEOSCCM.

The sensitivity of the stratospheric circulation to the air–sea roughness parameterization highlights the complexities in the atmospheric system. While it is difficult to conclusively isolate our mechanism linking air–sea roughness to stationary waves in a comprehensive chemistry–climate model, it is remarkable that a relatively simple change in the surface-layer parameterization leads to such an improvement in the stratospheric circulation. As many other CCMs use similar schemes for their air–sea roughness parameterization and have similar biases in the stratosphere (and also in Southern Ocean winds; Son et al. 2010, their Fig. 10), the results from GEOSCCM may be relevant to other models as well.

REFERENCES

Arblaster, J. M., and G. A. Meehl, 2006: Contributions of external forcings to southern annular mode trends. *J. Climate,* **19,** 2896–2905.

Barnes, E. A., and D. Hartmann, 2010a: Dynamical feedbacks and the persistence of the NAO. *J. Atmos. Sci.,* **67,** 851–865.

——, and ——, 2010b: Dynamical feedbacks of the southern annular mode in winter and summer. *J. Atmos. Sci.,* **67,** 2320–2330.

——, and C. I. Garfinkel, 2012: Barotropic impacts of surface friction on eddy kinetic energy and momentum fluxes: An alternative to the barotropic governor. *J. Atmos. Sci.,* **69,** 3028–3039.

Bodeker, G. E., B. J. Connor, J. B. Liley, and W. A. Matthews, 2001: The global mass of ozone: 1978-1998. *Geophys. Res. Lett.,* **28,** 2819–2822.

——, H. Shiona, and H. Eskes, 2005: Indicators of Antarctic ozone depletion. *Atmos. Chem. Phys.,* **5,** 2603–2615.

Branscome, L. E., W. J. Gutowski Jr., and D. A. Stewart, 1989: Effect of surface fluxes on the nonlinear development of baroclinic waves. *J. Atmos. Sci.,* **46,** 460–475.

Butchart, N., and Coauthors, 2011: Multimodel climate and variability of the stratosphere. *J. Geophys. Res.,* **116,** D05102, doi:10.1029/2010JD014995.

Chang, E. K. M., Y. Guo, X. Xia, and M. Zheng, 2013: Storm-track activity in IPCC AR4/CMIP3 model simulations. *J. Climate,* **26,** 246–260.

Charney, J. G., and P. G. Drazin, 1961: Propagation of planetary-scale disturbances from the lower into the upper atmosphere. *J. Geophys. Res.,* **66,** 83–109.

Chen, G., I. M. Held, and W. A. Robinson, 2007: Sensitivity of the latitude of the surface westerlies to surface friction. *J. Atmos. Sci.,* **64,** 2899–2915.

Chou, S.-H., E. Nelkin, J. Ardizzone, R. M. Atlas, and C.-L. Shie, 2003: Surface turbulent heat and momentum fluxes over global oceans based on the Goddard satellite retrievals, version 2 (GSSTF2). *J. Climate,* **16,** 3256–3273.

Edmon, H. J., B. J. Hoskins, and M. E. McIntyre, 1980: Eliassen–Palm cross sections for the troposphere. *J. Atmos. Sci.,* **37,** 2600–2616.

Garfinkel, C. I., and D. L. Hartmann, 2011: The influence of the quasi-biennial oscillation on the troposphere in wintertime in a hierarchy of models. Part II: Perpetual winter WACCM runs. *J. Atmos. Sci.,* **68,** 1214–1233.

——, ——, and F. Sassi, 2010: Tropospheric precursors of anomalous Northern Hemisphere stratospheric polar vortices. *J. Climate,* **23,** 3282–3299.

——, A. M. Molod, L. Oman, and I.-S. Song, 2011: Improvement of the GEOS-5 AGCM upon updating the air–sea roughness parameterization. *Geophys. Res. Lett.,* **38,** L18702, doi:10.1029/2011GL048802.

——, D. W. Waugh, and E. Gerber, 2012: Effect of tropospheric jet latitude on coupling between the stratospheric polar vortex and the troposphere. *J. Climate,* **26,** 2077–2095.

Held, I. M., 1975: Momentum transport by quasi-geostrophic eddies. *J. Atmos. Sci.,* **32,** 1494–1496.

Helfand, H. M., and S. D. Schubert, 1995: Climatology of the simulated Great Plains low-level jet and its contribution to the continental moisture budget of the United States. *J. Climate,* **8,** 784–806.

Holton, J. R., 2004: *An Introduction to Dynamic Meteorology.* Academic Press, 535 pp.

Hoskins, B. J., and K. I. Hodges, 2005: A new perspective on Southern Hemisphere storm tracks. *J. Climate,* **18,** 4108–4129.

Hurwitz, M. M., P. A. Newman, F. Li, L. D. Oman, O. Morgenstern, P. Braesicke, and J. A. Pyle, 2010: Assessment of the breakup of the Antarctic polar vortex in two new chemistry-climate models. *J. Geophys. Res.,* **115,** D07105, doi:10.1029/2009JD012788.

James, I. N., 1987: Suppression of baroclinic instability in horizontally sheared flows. *J. Atmos. Sci.,* **44,** 3710–3720.

——, and L. J. Gray, 1986: Concerning the effect of surface drag on the circulation of a baroclinic planetary atmosphere. *Quart. J. Roy. Meteor. Soc.,* **112,** 1231–1250, doi:10.1002/qj.49711247417.

Kidston, J., and G. K. Vallis, 2012: The relationship between the speed and the latitude of an eddy-driven jet in a stirred barotropic model. *J. Atmos. Sci.,* **69,** 3251–3263.

Matsuno, T., 1970: Vertical propagation of stationary planetary waves in the winter Northern Hemisphere. *J. Atmos. Sci.,* **27,** 871–883.

McLandress, C., T. G. Shepherd, S. Polavarapu, and S. R. Beagley, 2012: Is missing orographic gravity wave drag near 60°S the cause of the stratospheric zonal wind biases in chemistry–climate models? *J. Atmos. Sci.,* **69,** 802–818.

Molod, A., L. Takacs, M. Suarez, J. Bacmeister, I.-S. Song, and A. Eichmann, 2012: The GEOS-5 atmospheric general circulation model: Mean climate and development from MERRA to Fortuna. GMAO Tech. Rep. Series on Global Modeling and Data Assimilation 28, 124 pp. [Available online at https://gmao.gsfc.nasa.gov/pubs/docs/Molod484.pdf.]

——, M. Suarez, and G. Partyka, 2013: The impact of limiting ocean roughness on GEOS-5 AGCM tropical cyclone forecasts. *Geophys. Res. Lett.,* **40,** 411416, doi:10.1029/2012GL053979.

Pawson, S., R. S. Stolarski, A. R. Douglass, P. A. Newman, J. E. Nielsen, S. M. Frith, and M. L. Gupta, 2008: Goddard Earth Observing System chemistry-climate model simulations of stratospheric ozone-temperature coupling between 1950 and 2005. *J. Geophys. Res.,* **113,** D12103, doi:10.1029/2007JD009511.

Polvani, L. M., D. W. Waugh, G. J. P. Correa, and S.-W. Son, 2011: Stratospheric ozone depletion: The main driver of twentieth-century atmospheric circulation changes in the Southern Hemisphere. *J. Climate,* **24,** 795–812.

Rienecker, M. M., and Coauthors, 2008: The GEOS-5 data assimilation system—Documentation of versions 5.0.1, 5.1.0, and 5.2.0. GMAO Tech. Rep. Series on Global Modeling and Data Assimilation 27, 118 pp. [Available online at http://gmao.gsfc.nasa.gov/pubs/docs/Rienecker369.pdf.]

——, and Coauthors, 2011: MERRA: NASA's Modern-Era Retrospective Analysis for Research and Applications. *J. Climate,* **24,** 3624–3648.

Robinson, W. A., 1997: Dissipation dependence of the jet latitude. *J. Climate,* **10,** 176–182.

Scott, R. K., and P. H. Haynes, 2002: The seasonal cycle of planetary waves in the winter stratosphere. *J. Atmos. Sci.,* **59,** 803–822.

Smith, K. L., and P. J. Kushner, 2012: Linear interference and the initiation of extratropical stratosphere-troposphere interactions. *J. Geophys. Res.,* **117,** D13107, doi:10.1029/2012JD017587.

Son, S.-W., and Coauthors, 2010: Impact of stratospheric ozone on Southern Hemisphere circulation change: A multimodel assessment. *J. Geophys. Res.,* **115,** D00M07, doi:10.1029/2010JD014271.

SPARC-CCMVal, 2010: Stratospheric processes and their role in climate. SPARC Rep. 5, WCRP-132, WMO/TD-No. 1526, 609 pp.

Stolarski, R. S., A. R. Douglass, M. Gupta, P. A. Newman, S. Pawson, M. R. Schoeberl, and J. E. Nielsen, 2006: An ozone increase in the Antarctic summer stratosphere: A dynamical response to the ozone hole. *Geophys. Res. Lett.,* **33,** L21805, doi:10.1029/2006GL026820.

Taguchi, M., and S. Yoden, 2002: Internal interannual variability of the troposphere–stratosphere coupled system in a simple global circulation model. Part I: Parameter sweep experiment. *J. Atmos. Sci.,* **59,** 3021–3036.

Uppala, S. M., and Coauthors, 2005: The ERA-40 Re-Analysis. *Quart. J. Roy. Meteor. Soc.,* **131,** 2961–3012.

Vallis, G. K., 2006: *Atmospheric and Oceanic Fluid Dynamics: Fundamentals and Large-Scale Circulation.* Cambridge University Press, 745 pp.